Heavy ion fusion: Possible dynamical solution of the problem of the abnormally large diffuseness of the nucleus-nucleus potential

M. V. Chushnyakova and I. I. Gontchar
Physics and Chemistry Department, Omsk State Transport University, Omsk, Russia
(Received 16 October 2012; published 22 January 2013)

We attempt to make some progress in the problem of the apparently large diffuseness of the Woods-Saxon strong nucleus-nucleus interaction potential (SnnP) needed to fit a large number of precision fusion excitation functions. This problem has been formulated in Newton *et al.* [Phys. Lett. B **586**, 219 (2004); Phys. Rev. C **70**, 024605 (2004)]. We applied the classical dissipative trajectory model to describe the data on fusion (capture) of ^{16}O with ^{92}Zr, ^{144}Sm, and ^{208}Pb. No fluctuations or dynamical deformations of the interacting nuclei are accounted for. The friction force is supposed to be proportional to the squared derivative of the SnnP (the surface friction model). The SnnP is calculated within the framework of the double-folding model with the density-dependent M3Y NN forces. This potential is known to possess rather small diffuseness in contradistinction to what is required by the data analysis in Newton *et al.* [Phys. Lett. B **586**, 219 (2004); Phys. Rev. C **70**, 024605 (2004)]. Varying slightly the strength of radial friction (universally for all three reactions) and the diffuseness of the charge density of ^{208}Pb we have obtained satisfactory agreement of the calculated excitation functions with the data.

DOI: 10.1103/PhysRevC.87.014614 PACS number(s): 25.70.Jj, 25.60.Pj, 24.10.−i

I. INTRODUCTION

During last two decades an enormous amount of experimental data have been accumulated on the cross sections of the processes in which the collision of two complex nuclei (heavy ions) results in the formation of a single excited object [1,2]. In its consequent evolution, it does not necessarily pass through the spherical shape. The decay channels are very different: fission, quasifission, and neutron, light charged particle, and γ emission. The unifying signature of such reactions is that the decay products in the center-of-mass frame are emitted isotropically. This means that the dinuclear system (or the mononucleus) rotates several times before decaying. Considering the process from the theoretical point of view, one says that the fictitious particle with the reduced mass is captured in the potential pocket of the entrance channel. It seems natural to call the corresponding cross sections the capture cross sections. These are the cross sections which are referred to as the fusion cross sections in Ref. [1].

The capture cross sections are usually analyzed within the framework of the coupled-channels model [3,4]. The nucleus-nucleus strong interaction potential (SnnP) is the key element of this model. Conventionally, the Woods-Saxon (WS) ansatz

$$U_n(R) = V_{\rm WS}\left\{1+\exp\left[\frac{R-r_{\rm WS}\left(A_P^{1/3}+A_T^{1/3}\right)}{a_{\rm WS}}\right]\right\}^{-1} \qquad (1)$$

is used as the SnnP in the coupled-channels calculations. In Eq. (1) R denotes the distance between the centers of mass of two spherical nuclei: the projectile with the mass number A_P and the target of the mass number A_T. The WS potential is defined by three parameters: the depth $V_{\rm WS}$, the radius parameter $r_{\rm WS}$, and the diffuseness $a_{\rm WS}$. Systematic analysis of the experimental capture excitation functions in Ref. [1] demonstrated that the values of $a_{\rm WS}$ ranging between 0.75 and 1.5 fm are needed to reproduce those functions. This is much larger than the value of 0.65 fm, which is required by the elastic scattering data. It was pointed out in Ref. [1] that these abnormally large diffusenesses might be an artifact masking some dynamical effects.

Following this idea, we undertake an effort to analyze the experimental capture excitation functions using the simplest dynamical model: the classical dissipative trajectory model with the surface friction [5]. This model was first proposed in Ref. [6] and developed later in Refs. [7–9].

In Ref. [6] only the conservative and dissipative forces between the colliding nuclei were accounted for. The nuclei were considered to be solid spheres. Two collective variables characterized the motion of the system: the center-of-mass distance R and the rotation angle φ. The dissipative forces were taken to be proportional to the squared derivative of the SnnP. The authors of Ref. [6] managed to find a universal (i.e., system independent) parameter set making it possible to reproduce about 20 experimental capture excitation functions.

In Ref. [8] the model was supplemented with the dynamical quadrupole deformations of the colliding nuclei. Within the framework of this refined model it turned out to be possible to reproduce satisfactorily about 100 experimental capture excitation functions with typical agreement of about 20%. For this aim again a universal parameter set was used which was close to the one of Ref. [6].

Further modification of the model [8] was done in Refs. [7,9,10], where the thermal fluctuations of all the variables were taken into consideration. This modification forced the authors to revise the capture criterion. The comparison with the experiment, although rather successful, was performed in this version of the model for a significantly smaller number of reactions (less than 10).

In Refs. [6,7,9,10] the SnnP was calculated by means of folding the nucleus-nucleon optical potential with the nucleon density (single-folding). Nowadays, a more elaborated double-folding (DF) SnnP with the density-dependent M3Y NN forces [11,12] is available. Moreover, the data analyzed in Refs. [6,7,9,10] typically had an accuracy worse than 10%. Presently, high-precision data (typically 1%) have been

accumulated (see, e.g., Refs. [13–15]). So, it is tempting to analyze these new data with the DF potential to see whether accounting for the dynamical effects can resolve the problem of the apparently large diffuseness. This is what we aim to explore in the present work.

The paper is organized as follows. In Sec. II the model is described with the emphasis on the potential energy and its approximation by the analytical formulas. Here the initial and capture conditions are also discussed. In Sec. III the impact of the model parameter variation on the calculated capture excitation functions is studied and the comparison with earlier work is made. Our resulting cross sections are compared with the experimental data in Sec. IV. In Sec. V the conclusions are drawn.

II. DESCRIPTION OF THE MODEL

Within the framework of the classical (nonquantum) dissipative trajectory model [6], the fictitious particle with the reduced mass moves experiencing the action of the conservative and dissipative forces. Despite the description of the model can be found in Ref. [6], we prefer to give all the equations to help in reading and understanding the results. We also modify some relations of the model.

A. Equations of motion

The level of complexity of the model is dictated by the data the model is designed to describe. Because the problem of the apparently large diffuseness of the SnnP appears at rather high incident energy it seems unnecessary to account for quantum effects like tunneling. For our exploratory work we choose three experimental precision capture excitation functions: ^{16}O + ^{92}Zr [13], ^{16}O + ^{144}Sm [14], and ^{16}O + ^{208}Pb [15]. All nuclei involved in these reactions are spherical and rather stiff owing to their closed shells. That is why we account only for two degrees of freedom corresponding to the radial and orbital motion. The dimensionless coordinates are $q = R/R_{PT}$ and φ. The latter is the angle between the line connecting the center of force with the fictitious particle at the given time moment and the linear momentum of the fictitious particle at $q \gg 1$. Here R is the distance between the centers of the colliding nuclei and R_{PT} is equal to the sum of the half-density radii: $R_{PT} = R_P + R_T$ (P and T denote the projectile and target nuclei, respectively).

The equations of motion read

$$\Delta p = (F_U + F_{\rm cen} + F_{Dq})h_t, \tag{2a}$$

$$\Delta q = \frac{p}{m_q}h_t, \tag{2b}$$

$$\Delta L = F_{D\varphi}h_t, \tag{3a}$$

$$\Delta \varphi = \frac{\hbar L}{m_q}h_t \tag{3b}$$

$$F_U = -\frac{dU_{\rm tot}}{dq}, \tag{4a}$$

$$F_{\rm cen} = \frac{\hbar^2 L^2}{m_q q^3}, \tag{4b}$$

$$F_{Dq} = -\frac{p}{m_q}K_R\left(\frac{dU_n}{dq}\right)^2, \tag{5a}$$

$$F_{D\varphi} = -\frac{(L - L_s)}{m_q}K_\varphi\left(\frac{dU_n}{dq}\right)^2. \tag{5b}$$

Here p stands for the linear momentum corresponding to the radial motion ($[p] = $ MeV zs); F_U and $F_{\rm cen}$ are the conservative and centrifugal forces, respectively; F_{Dq} and $F_{D\varphi}$ are the dissipative forces corresponding to the radial and orbital motion, respectively. $U_{\rm tot}(q)$ is the total interaction energy of two nuclei which consists of the Coulomb $U_C(q)$ and SnnP $U_n(q)$ parts ($[U] = $ MeV); $\hbar L$ is the projection of the orbital angular momentum onto the axis perpendicular to the reaction plane ($[\hbar] = $ MeV zs); $m_q = m_n A_P A_T R_{PT}^2 (A_P + A_T)^{-1}$ is the radial inertia parameter ($[m_q] = $ MeV zs^2); m_n is the bare nucleon mass; K_R denotes the coefficient defining the strength of dissipation of the radial motion ($[K_R] = $ MeV^{-1} zs); h_t is the time step of the computer modeling ($[h_t] = $ zs); K_φ denotes the coefficient defining the strength of dissipation of the orbital angular momentum ($[K_\varphi] = $ MeV^{-1} zs). $L_s = 7L_0/5$ stands for the value of the orbital quantum number to which L is relaxing during its evolution (when L becomes equal to L_s the dinuclear system rotates as the solid body). Note that L_s is present in Refs. [7] [Eq. (9)], [8] [Eq. (3)], and [16] [Eq. (4)] and is absent in Refs. [5] [Eq. (12.13)], [6] [Eq. (2.3)], [9] [Eq. (1)], and [10] [Eq. (69)]. Equations (2) and (3) are solved using the Runge-Kutta method of the fourth order.

Of course, our model is very simple with regard to the dynamics because it does not account for the dynamical deformations of the colliding nuclei and the thermal fluctuations of the collective variables. However, we prefer first to be certain about the role of the potential and friction in failure or success in resolving the apparently large diffuseness problem in the description of the capture excitation function. We do not expect the above-mentioned deformations and fluctuations play the decisive role in that.

B. Dynamical trajectories

It is instructive to see the dynamical behavior of the fictitious particle in the cases of capture and reflection from the barrier. This is illustrated in Fig. 1, where the time dependence of the radial coordinate [Fig. 1(a)], the radial momentum [Fig. 1(b)], the dissipative radial force [Fig. 1(c)], and the dissipated energy [Fig. 1(d)] are shown. The collision ^{16}O +^{144} Sm at the angular momentum $L = 8$ and four values of the center-of-mass energy (55 MeV, particle 1; 60 MeV, particle 2; 62 MeV, particle 3; 67 MeV, particle 4) were selected as the representative examples. The barrier height is $U_{B8} = 60.4$ MeV, its dimensionless radius $q_{B8} = 1.31$ [it is shown by the horizontal line in Fig. 1(a)].

In Figs. 1(a) and 1(b) it is seen that particle 1 is reflected from the barrier significantly below its summit. The second particle is reflected as well but spends somewhat longer time near the barrier. These particles move almost uniformly accelerated because the dissipative forces are small and the motion proceeds near the turning point.

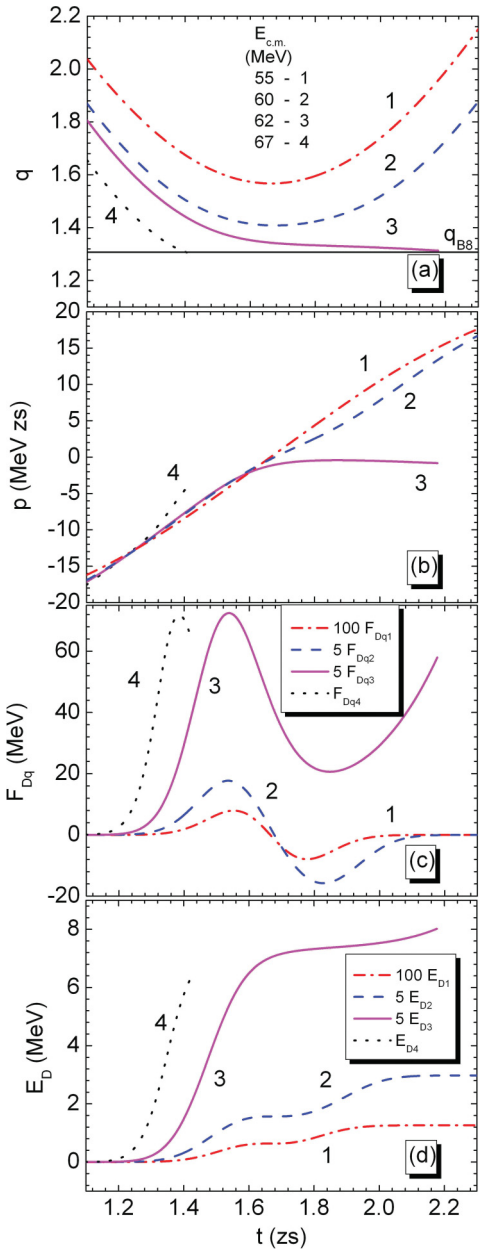

FIG. 1. (Color online) The time dependence of the radial coordinate q (a), the radial momentum p (b), the dissipative radial force F_{Dq} (c), and the dissipated energy E_D (d) for four trajectories corresponding to the reaction $^{16}O + ^{144}Sm$ at different values of $E_{c.m.} = 55, 60, 62, 67$ MeV ($L = 8$). The calculations are performed using the GK approximation of the DF2 potential (for details, see Sec. II D).

Particle 3 loses almost all of its kinetic energy as it comes to the barrier top. Beginning from $t = 1.5$ zs it moves very slowly, creeping to the point of capture (the capture conditions are specified in part E of this section). The fourth particle overcomes the barrier and still possesses significant linear momentum.

The dissipative forces and the dissipated energies are substantially different for our four particles. That is why these quantities are multiplied by a factor of 5 for the second and the third particles and by a factor of 100 for the fourth one. Comparing Figs. 1(a) and 1(d) we see that the dissipative force appears at approximately $q = 1.6$. The nonmonotonic behavior of the dissipative force in Fig. 1(c) is explained by its structure [see Eq. (5a)]. This force increases as the particle comes closer to the force center owing to the form factor. However, the particle velocity decreases and finally the force goes down.

Let us discuss a bit in detail the reflected particles 1 and 2. For them the dissipative force changes the sign at the turning point. In Fig. 1(d) the two regions where the dissipated energy increases are clearly seen. The regions coincide with the locations of the extremes of F_{Dq} in Fig. 1(c). The absolute values of both F_{Dq} and E_D are very small (for the particle 1 by factor of 100 smaller than it appears in the figures) but the behavior of these quantities is correct and understandable. This corroborates our confidence that the division of the particles into reflected and captured is correct.

C. Temperature

The temperature does not enter explicitly Eqs. (2) and (3). However, the colliding nuclei must heat up and their temperature tells us about the dissipated energy. Moreover, the temperature enters the capture condition [see Eq. (27)].

Following Refs. [7,9,10] we assume that the colliding nuclei are in thermal equilibrium with each other. Thus, the dinuclear system is characterized by the only temperature θ. In Refs. [7,9,10] the temperature was calculated using the Fermi-gas equation of state:

$$\theta = \sqrt{\alpha E_{DP(T)} A_{P(T)}^{-1}}. \tag{6}$$

Here $E_{DP(T)}$ is the intrinsic excitation energy of the projectile (target) nucleus. This energy coincides with the dissipated energy of the collective motion shared by the particular nucleus. When Eq. (6) is used the dissipated energy is divided between the reagents proportionally to their mass numbers.

It is well known, however (see, e.g., Refs. [5,10,17,18]), that the single-particle level density parameter is not a linear function of the mass number. Thus, we use the following equation:

$$\theta = \sqrt{E_{DP(T)}\left(a_1 A_{P(T)} + a_2 A_{P(T)}^{2/3}\right)^{-1}}, \tag{7}$$

where $a_1 = 0.073$ MeV^{-1} and $a_2 = 0.095$ MeV^{-1} [17]. In this case the dissipated energy is pumped from the heavy nucleus to the light one compared to the case of Eq. (6). The energy change can reach 10% for the light nucleus.

D. Potential energy

In Refs. [6–10] the SnnP was calculated by means of folding the nucleus-nucleon optical potential with the nucleon density (the symmetrized single-folding potential). In the present work we use the following potentials and their approximations:

(i) the WS potential with the parameters fitted to reproduce the large number of precision fusion excitation

functions using the single barrier penetration model (BPM) [1];

(ii) the DF potential with zero radius exchange forces (DFz);

(iii) the DF potential with the finite radius exchange forces without the density dependence of the NN forces (DF0);

(iv) the DF potential with the finite radius exchange forces with the density dependent NN forces (DF2);

(v) the analytical approximation of the symmetrized single-folding potential (Gross-Kalinowski formula [6], GK formula),

$$U_n(R) = \ln\left\{1+\exp\left(-\frac{\Delta R}{a_{\rm GK}}\right)\right\} \times [A_{0\rm GK} + A_{1\rm GK}\Delta R + A_{2\rm GK}\Delta R^2], \quad (8)$$

$$\Delta R = R - r_{\rm GK}\left(A_P^{1/3} + A_T^{1/3}\right), \quad (9)$$

$$r_{0\rm GK} = 1.30 \text{ fm}, \quad a_{\rm GK} = 0.61 \text{ fm}, \quad A_{0\rm GK} = 33 \text{ MeV},$$
$$A_{1\rm GK} = 2 \text{ MeV}, \quad A_{2\rm GK.} = 3 \text{ MeV}. \quad (10)$$

Note that in the original GK formula of Ref. [6] there are two more terms in the polynomial; however, the authors claimed that these extra terms are not of importance to obtain good fit of the symmetrized single-folding potential "all over the periodic table."

The description of the DF potential can be found in many papers (see, e.g., Refs. [11,19]). Presently the code designed to calculate the nucleus-nucleus interaction energy for two spherical nuclei is available [12]. Let us stress that in these papers the option of the finite-range density-dependent NN forces is included. The DF SnnP consists of the direct U_{nD} and the exchange U_{nE} parts:

$$U_n(R, E_P) = U_{nD}(R, E_P) + U_{nE}(R, E_P). \quad (11)$$

The direct part reads

$$U_{nD}(R, E_P) = g(E_P)\int d\vec{r}_P \int d\vec{r}_T\, \rho_{AP}(\vec{r}_P) F_{\rm v}(\rho_{FA}) {\rm v}_D(s) \rho_{AT}(\vec{r}_T). \quad (12)$$

Here the vector $\vec{s} = \vec{R} + \vec{r}_T - \vec{r}_P$ corresponds to the distance between two specified interacting points of the projectile and target nuclei, whose radius vectors are $\vec{r}_P$ and $\vec{r}_T$, respectively; ρ_{AP} and ρ_{AT} are the distributions of the nucleon centers of mass (the nucleon densities) at the ground state of the colliding nuclei, ${\rm v}_D$ is the direct part of the effective nuclear interaction between two nucleons. The multiplier $g(E_P)$ reflects the additional (explicit) collision energy dependence of the potential and depends upon the energy per nucleon $E_P = E_{\rm lab}/A_P$. It reads

$$g(E_P) = 1 - k_g E_P. \quad (13)$$

The function $F_{\rm v}(\rho_{FA})$ is responsible for the density dependence of the NN interaction according to Ref. [11]:

$$F_{\rm v}(\rho_{FA}) = C_{\rm v}\{1 + \alpha_{\rm v}\exp(-\beta_{\rm v}\rho_{FA}) - \gamma_{\rm v}\rho_{FA}\}. \quad (14)$$

The argument of this function corresponds to the density at the midpoint between two interacting nucleons and reads

$$\rho_{FA} = \rho_{AP}(\vec{r}_P + \vec{s}/2) + \rho_{AT}(\vec{r}_T - \vec{s}/2). \quad (15)$$

The exchange part of the nuclear interaction has the form

$$U_{nE}(R, E_P) = g(E_P)\int d\vec{r}_P \int d\vec{r}_T\, \rho_{AP}(\vec{r}_P; \vec{r}_P + \vec{s}) \times F_{\rm v}(\rho_{FA}) {\rm v}_E(s) \rho_{AT}(\vec{r}_T; \vec{r}_T - \vec{s}) \times \exp(i\vec{k}_{\rm rel}\vec{s}\, m_n/m_R). \quad (16)$$

Here ${\rm v}_E$ is the exchange part of the effective NN interaction.

In the present work we use the Paris NN forces [20]. They comprise a sum of the Yukawa-type terms, known as the M3Y effective NN interaction, for both the direct ${\rm v}_D$ and the exchange ${\rm v}_{Ef}$ parts:

$${\rm v}_D(s) = \sum_{i=1}^{3} G_{Di}[\exp(-s/r_{{\rm v}i})]/(s/r_{{\rm v}i}), \quad (17)$$

$${\rm v}_{Ef}(s) = \sum_{i=1}^{3} G_{Efi}[\exp(-s/r_{{\rm v}i})]/(s/r_{{\rm v}i}). \quad (18)$$

Here the subscript Ef refers to the finite-range exchange part of the NN interaction. Each term is determined by the radius parameters $r_{{\rm v}i}$ and the coefficients G_{Di} and G_{Efi}. In the case of the zero-range exchange NN interaction,

$${\rm v}_{E\delta}(\vec{s}) = G_{E\delta}\delta(\vec{s}). \quad (19)$$

The values of G_{Di}, G_{Efi}, $G_{E\delta}$, $r_{{\rm v}i}$, and k_g are collected in Table I.

Different approximations are used for describing the nuclear densities. The most widespread ansatz is the WS profile [21–24],

$$\rho_{AP(T)}(r) = \rho_{0P(T)}\left\{1+\exp\left(\frac{r - R_{P(T)}}{a_{P(T)}}\right)\right\}^{-1}. \quad (20)$$

Here $\rho_{0P(T)}$ is the parameter extracted from the normalization condition, the diffuseness parameter $a_{P(T)}$ defines a surface layer thickness, and $R_{P(T)}$ is a half density radius.

The wave number $k_{\rm rel}$, associated with the relative motion of the colliding nuclei, reads

$$k_{\rm rel}(R) = \{2m_R[E_{\rm c.m.} - U_{\rm tot}(R)]/\hbar^2\}^{1/2}. \quad (21)$$

TABLE I. The parameters of the M3Y interactions in Eqs. (13) and (17)–(19).

G_{D1} (MeV)	11 062
G_{D2} (MeV)	−2537.5
G_{D3} (MeV)	0
G_{Ef1} (MeV)	−1524.25
G_{Ef2} (MeV)	−518.75
G_{Ef3} (MeV)	−7.847
$(r_{\rm v1})^{-1}$ (fm)	4.0
$(r_{\rm v2})^{-1}$ (fm)	2.5
$(r_{\rm v3})^{-1}$ (fm)	0.7072
$G_{E\delta}$ (MeV fm^3)	−592
k_g (MeV^{-1})	0.002

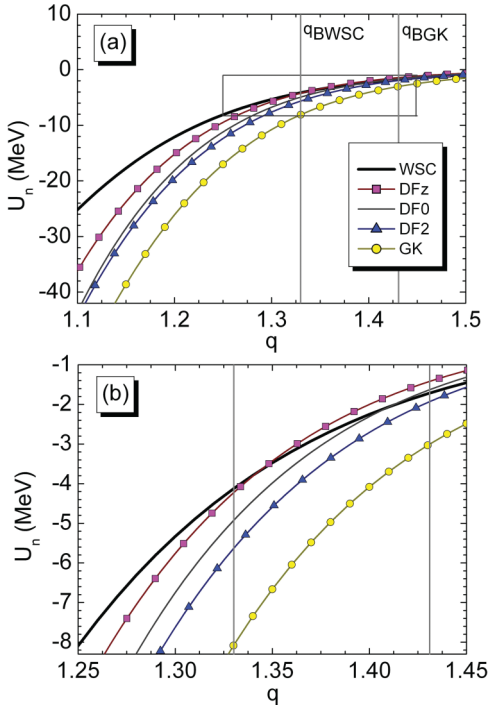

FIG. 2. (Color online) The SnnPs versus the dimensionless center-to-center distance for the reaction $^{16}O + ^{92}Zr$ with different scales (a) in general and (b) in details [the box in (a) indicates the region displayed in (b)]. The vertical lines indicate the Coulomb barrier radii range. WSC, the WS potential with the parameters fitted by the Canberra group [1]; DFz, the DF potential with the zero-range NN interaction; DF0, the DF potential with the finite-range density independent NN interaction; DF2, the DF potential with the finite-range density dependent NN interaction; GK, the analytical profile fitting the single-folding potential (Gross-Kalinowski formula).

Equations (11), (16), and (21) result in a self-consistency problem. It is solved by the iterative procedure which converges rather quickly if, for instance, one takes the total potential without the exchange nuclear part at the first step. All the details of the DF potentials calculation can be found in Ref. [12].

Because the application of Eq. (19) is the simplest and the fastest way to calculate the DF potential, this version is used most often [22–27]. We denote this potential as DFz. A more realistic case is the DF potential with the density-independent finite range NN forces. We refer to this potential as to DF0. To avoid the violation of the nuclear-matter saturation condition, the NN interaction with the density dependence

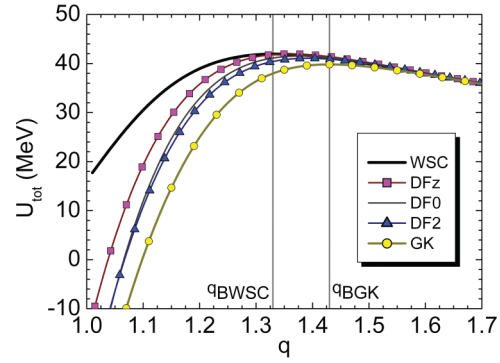

FIG. 3. (Color online) Total nucleus-nucleus potentials calculated for $L = 0$ versus the dimensionless center-to-center distance for the system $^{16}O + ^{92}Zr$. The notations are as in Fig. 2.

was introduced in Ref. [28]. In Ref. [19] it was shown that the Coulomb barrier (and consequently the potential itself) calculated using the set of the density-dependence parameters DD2 ($C_v = 0.3429$, $\alpha_v = 3.0232$, $\beta_v = 3.5512$ fm^{-3}, $\gamma_v = 0.5$ fm^{-3}) has the largest difference against the one calculated without the density dependence. In the present work we denote this potential as DF2. These are the three versions of the DF potential we use.

The five potentials (WSC, DFz, DF0, DF2, and GK) calculated for the $^{16}O + ^{92}$ Zr reaction are shown in Fig. 2. The vertical lines indicate the range of the barrier radii. Their values as well as other parameters used in these calculations are collected in Table II. It is seen in Fig. 2(a) that the effective diffusenesses of all three DF potentials are intermediate between those of the GK and WSC potentials. Because the DF potentials are very close to each other in Fig. 2(a), we show the potentials in Fig. 2(b) more in detail. One can conclude from this figure that the barriers should range as follows: $U_{BL}(DF2) < U_{BL}(DF0) < U_{BL}(DFz)$. This is in accord with Table II.

Let us note that among the five potentials in Fig. 2 the WSC and GK potentials provide the upper and lower limits. These are the two potentials using which good agreement with the data was obtained in Refs. [1] and [6], respectively. This observation supports the idea that the apparently large diffuseness of the SnnP seems to be an artifact.

It is interesting to inspect the total nucleus-nucleus potentials calculated with the parameters of Table II. The potentials are shown in Fig. 3 for zero angular momentum. A remarkable feature of the potentials is that none of them provides a pocket. In some works (see, e.g., Refs. [23,29]) its absence

TABLE II. Parameters of the potentials for the system $^{16}O + ^{92}Zr$ displayed in Figs. 2–10, 12, and 13.

Potential	q_{B0}	R_{B0} (fm)	U_{B0} (MeV)	Parameters of the potential
WSC	1.330	10.00	41.94	$a_{WS} = 0.841$ fm, $r_{WS} = 1.046$ fm, $V_{WS} = -100.0$ MeV [1]
DFz	1.360	10.23	41.96	$A_0 = 21.5$ MeV, $A_1 = 3.2$ MeV, $A_2 = 0.0$ MeV, $r_0 = 1.28$ fm, $a = 0.60$ fm
DF0	1.377	10.36	41.51	$A_0 = 21.0$ MeV, $A_1 = 3.4$ MeV, $A_2 = 0.2$ MeV, $r_0 = 1.30$ fm, $a = 0.58$ fm
DF2	1.392	10.47	41.06	$A_0 = 20.5$ MeV, $A_1 = 4.8$ MeV, $A_2 = 4.4$ MeV, $r_0 = 1.32$ fm, $a = 0.50$ fm
GK	1.430	10.76	39.81	As in Eq. (10)
DFz, DF0, DF2				$R_P = 2.608$ fm, $a_P = 0.465$ fm, $R_T = 4.913$ fm, $a_T = 0.533$ fm [19]

TABLE III. Parameters of the potentials for the system $^{16}O + ^{144}Sm$ displayed in Figs. 1, 6, 10, and 12.

Potential	q_{B0}	R_{B0} (fm)	U_{B0} (MeV)	Parameters of the potential
WSC	1.30	10.84	61.09	$a_{WS} = 0.75$ fm, $r_{WS} = 1.108$ fm, $V_{WS} = -100.0$ MeV [1]
DFz	1.31	10.88	61.25	$R_P = 2.608$ fm, $a_P = 0.465$ fm; $R_T = 5.719$ fm, $a_T = 0.557$ fm [19]; $A_0 = 21.5$ MeV, $A_1 = 4.6$ MeV, $A_2 = 1.2$ MeV, $r_0 = 1.28$ fm, $a = 0.56$ fm
DF2	1.34	11.17	59.83	$A_0 = 20.0$ MeV, $A_1 = 4.6$ MeV, $A_2 = 4.6$ MeV, $r_0 = 1.32$ fm, $a = 0.50$ fm

is considered as a disadvantage of the potential. In our opinion any SnnP calculated using the frozen density approximation (diabatic potential) is suitable only for $q > q_t$, where $q_t = 1$ is the contact radius (this is clearly stated in Ref. [8], p. 347). At this separation the nucleon density ρ_A in the overlap region reaches the value of saturation of $\rho_{As} = 0.17$ fm^{-3}. At $q < q_t$ an intensive redistribution of the charge and the mass must start, which is expected to be described by another potential. Consequently, the speculations on whether the entrance channel potential possesses a pocket or it does not are of little value.

The DF potential with the M3Y NN forces is known for about 30 years however, it seldom is used (if it is) for dynamical calculations of the capture cross sections. The trouble is that the integrals entering Eqs. (12) and (16) are difficult to be calculated accurately enough at the large values of q. The situation is illustrated by Fig. 4, where the SnnPs are shown in the logarithmic scale for the large values of separation. It is seen that already at $q > 2.2$ the DF potentials start to oscillate. These oscillations are of no importance for the BPM calculations where only the height and curvature of the barrier are needed. However, for the dynamical calculations the derivative of the potential is required which cannot be stable as the potential oscillates. Another thing we notice in Fig. 4 is that the WSC and GK potentials are less steep than the DF ones. This can result in smaller radial friction coefficient K_R needed to describe the capture data with the DF potentials compared to the case of the GK potential.

The standard way to circumvent the problem of the oscillations of the DF potential at $q > 2.2$ is to approximate the numerical potential by an analytical formula. In Ref. [19] the DF potential was fitted near the barrier by the WS formula (1). The relative accuracy of this fit turned out to be of order of 10^{-5}. This is enough to compute the capture cross sections using the BPM. However, a much wider range of separation influences the dynamical modeling. Using the formula, approximating the DF potential near the barrier, for calculations of the dissipative forces [see Eqs. (5)] one can be in error.

That is why we decided, in addition to the WS formula, to approximate the calculated DF potential by means of the GK formulas (8) and (9). The q-dependence of the DF potentials (solid lines) and their WS and GK approximations (dashed-dotted lines and dashed lines, respectively) are presented in Fig. 5. These calculations are done for the $^{16}O + ^{92}Zr$ reaction. The approximations are performed in the range $0.8q_{B0} < q < 1.2q_{B0}$. The barrier positions are indicated by the vertical lines. Near the barrier [Figs. 5(a), 5(c), 5(e)] the WS and GK fits are equally good. However, in the region of large separations [Figs. 5(b), 5(d), 5(f)] the GK approximation is certainly preferential.

For $q < q_{B0}$ [Figs. 5(a), 5(c), 5(e)] it is not that clear which approximation should be preferred. However, our dynamical trajectories seldom penetrate deeper than $q = 0.9q_{BL}$. Thus, everywhere below the GK approximations of the DF potentials are used.

E. Capture cross sections

The capture cross sections are calculated according to the commonly used formula (see, e.g., Ref. [18]):

$$\sigma = \frac{\pi\hbar^2}{2m_R E_{\text{c.m.}}} \sum_{L=0}^{L_{\max}} (2L+1)\, T_L. \tag{22}$$

Obviously, the values of the cross sections should not depend upon the value of the technical parameter $L_{\max}$. The transmission coefficients T_L are evaluated using two models: the classical dissipative trajectory model with the surface friction (TMSF) and the single BPM.

Within the framework of the TMSF the transmission coefficient can be equal to either 1 provided the trajectory corresponding to L is captured into the orbital motion or 0 otherwise. At $E_{\text{c.m.}} > U_{BLc}$ all the trajectories with L ranging

TABLE IV. Parameters of the potentials for the system $^{16}O + ^{208}Pb$ displayed in Figs. 6, 10, and 11.

Potential	q_{B0}	R_{B0} (fm)	U_{B0} (MeV)	Parameters of the potential
WSC	1.22	11.31	74.53	$a_{WS} = 1.11$ fm, $r_{WS} = 1.035$ fm, $V_{WS} = -100.0$ MeV [1]
DFz	1.25	11.53	76.70	$R_P = 2.608$ fm, $a_P = 0.465$ fm; $R_T = 6.631$ fm, $a_T = 0.505$ fm [19]; $A_0 = 20.0$ MeV, $A_1 = 4.8$ MeV, $A_2 = 3.2$ MeV, $r_0 = 1.28$ fm, $a = 0.50$ fm
DF2	1.27	11.75	75.28	$A_0 = 21.0$ MeV, $A_1 = 4.8$ MeV, $A_2 = 3.4$ MeV, $r_0 = 1.30$ fm, $a = 0.50$ fm

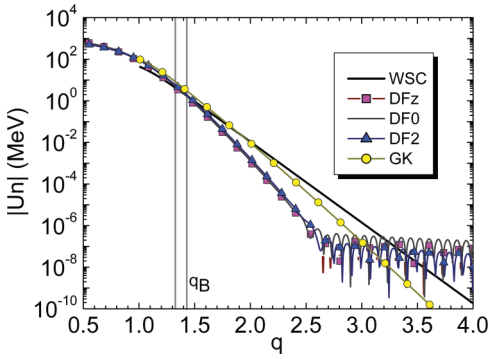

FIG. 4. (Color online) The absolute values of the SnnPs for the system $^{16}O + ^{92}Zr$ versus the dimensionless center-to-center distance in the logarithmic scale and for the wide range of q. The notations are as in Figs. 2 and 3.

from 0 up to L_c are captured. Let us stress that unlike Refs. [6,8,10] we keep our variable L (and consequently L_c) to be discrete in calculating the cross sections. Performing in Eq. (22) summation up to L_c we obtain

$$\sigma = \frac{\pi\hbar^2}{2m_R E_{\text{c.m.}}} L_c(L_c + 2). \tag{23}$$

Within the framework of the BPM using the parabolic barrier approximation the transmission coefficient reads [30]

$$T_L = \{1 + \exp[2\pi\,(U_{BL} - E_{\text{c.m.}})\,/\,(\hbar\omega_{BL})]\}^{-1}. \tag{24}$$

It was demonstrated in Ref. [1] that the experimental capture cross sections are reproduced with good accuracy by the BPM with the transmission coefficients (24) and the WS potential provided the collision energy is at least 5%–10% above the barrier. The depth of the WS potential was fixed $V_{\text{WS}} = -100$ MeV, whereas the radius and diffuseness were fitted individually for each reaction. We denote this potential as WSC (Woods-Saxon with the Canberra parameters).

The quality of the data reproduction by the BPM with different potentials is illustrated by Fig. 6. In addition to

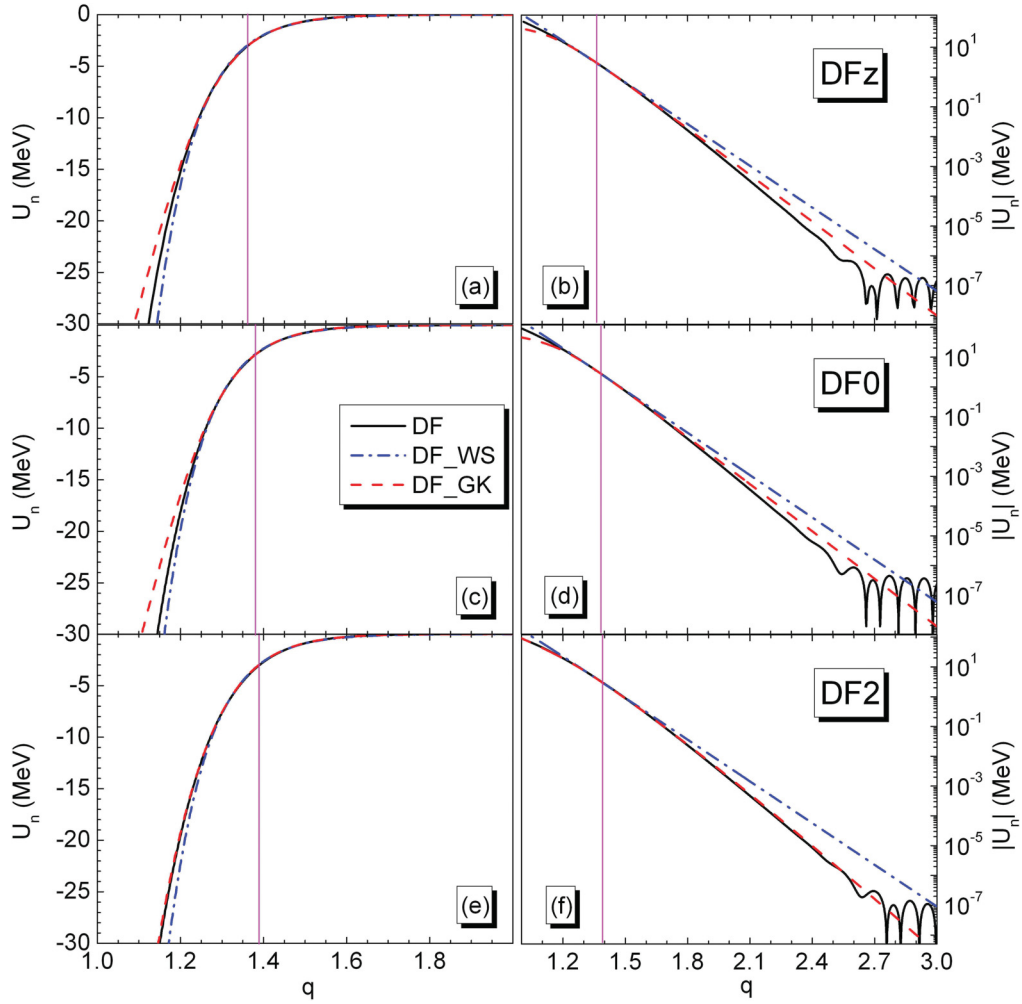

FIG. 5. (Color online) The absolute values of the SnnPs versus the dimensionless center-to-center distance for the reaction $^{16}O + ^{92}Zr$ in linear (a), (c), (e) and logarithmic (b), (d), (f) scales. The Woods-Saxon and the Gross-Kalinowski formula approximations for the double-folding potentials (denoted as DF_WS and DF_GK, respectively) are shown as well. The calculations are performed for three versions of the SnnP: DFz (a), (b), DF0 (c), (d), and DF2 (e), (f).

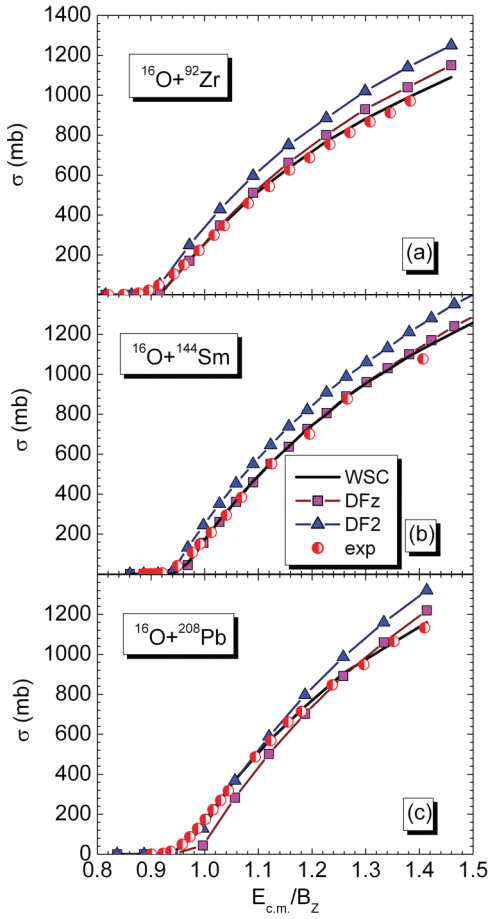

FIG. 6. (Color online) Experimental data for the fusion excitation functions (semiopen circles) for the systems $^{16}O + ^{92}Zr$ (a), $^{16}O + ^{144}Sm$ (b), and $^{16}O + ^{208}Pb$ (c) from Refs. [13–15], respectively, are compared with the results of our calculations made using the BPM. Thick lines without symbols correspond to the WSC potential; lines with solid symbols correspond to the GK approximation of the double-folding potentials (squares, DFz; triangles, DF2) $B_Z = Z_P Z_T/(A_P^{(1/3)} + A_T^{(1/3)})$. The parameters of the potentials are shown in Tables II–IV.

the experimental points (semiopen circles) and the results obtained using the WSC potential (solid line without symbols), shown in Fig. 6 are the cross sections calculated using the GK approximations of the DFz (squares) and DF2 (triangles) potentials. The error bars for the experimental data are inside the symbols. Remember that for the BPM calculations it does not matter which of the following to use: (i) the DF potential itself, (ii) the WS approximation of the DF potential, (iii) the GK approximation of the DF potential. One sees that whatever the DF potential is, the values of the calculated cross sections exceed the data at high collision energies. Moreover, the excitation functions calculated using the DF potentials are rising faster than the experimental ones. As we have seen in Fig. 2, the principal difference between the WSC and DF potentials consists of the large diffuseness of the former. Yet the DF2 potential is based on the well-founded microscopic effective M3Y density-dependent NN forces.

This is the essence of the problem of the apparently large diffuseness we are trying to tackle in our present work.

F. Initial and capture conditions

The dynamical calculations start from a final value of the radial coordinate q_0 and a particular value of L. Therefore, the initial value of the radial momentum is also L- and q_0-dependent through the energy conservation law:

$$p_{0L} = \sqrt{2m_q[E_{\text{c.m.}} - U_C(q_0) - U_n(q_0) - U_{\text{cen}}(q_0, L)]}. \quad (25)$$

The initial value of the radial coordinate q_0 is chosen to obey two conditions. First, it should not be too large to avoid slowing down calculations (especially considering in future accounting for fluctuations of the collective variables). Second, it should not be too close to the capture barrier; otherwise, the not accounted dissipative part of the trajectory can spoil the results. Obviously, the calculated cross sections should not depend on q_0. The excitation functions for the $^{16}O + ^{92}Zr$ reaction calculated at different values of q_0 are shown in Fig. 7. The GK potential is used for this particular example. We start to vary q_0 from 5.1 and move closer to the barrier. Figure 7(a) shows that in the range $3.5 < q_0 < 5.1$ the excitation function does not exhibit any regular variations. There are some rare jumps owing to the bifurcation of the single partial wave. To prove this we plot the cross sections [Fig. 8(a)] and the corresponding L_c values [Fig. 8(b)] calculated at four values of $E_{\text{c.m.}}$ as functions of q_0. Now the jumps are seen in detail between $q_0 = 4.5$ and $q_0 = 3.5$ on the curves corresponding to $E_{\text{c.m.}} = 51.4$ and 47.0 MeV. They occur owing to a tiny

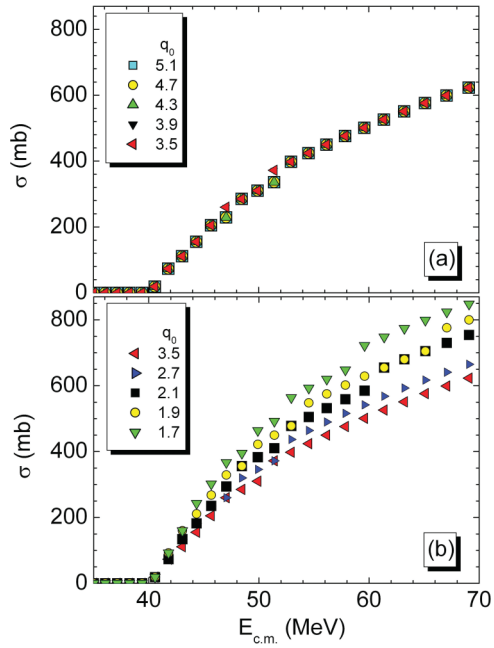

FIG. 7. (Color online) The capture excitation functions for the different initial values of the radial coordinate q_0 for the reaction $^{16}O + ^{92}Zr$ [TMSF, GK potential of Eqs. (8)–(10)].

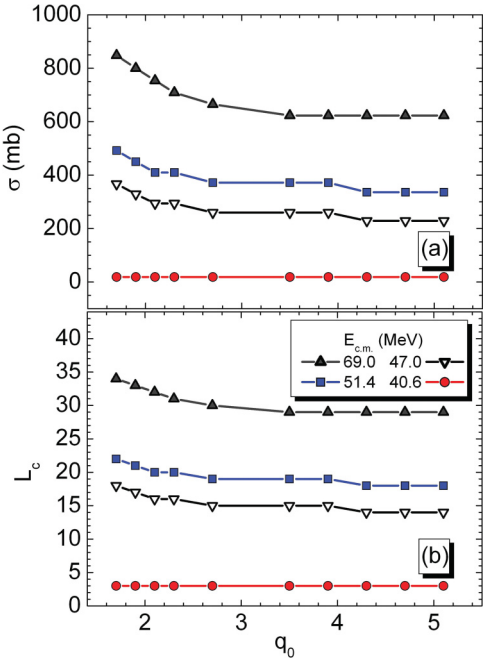

FIG. 8. (Color online) The capture cross sections (a) and L_c (b) versus the initial values of the radial coordinate q_0 for four different values of $E_{\text{c.m.}}$. It is the same calculation as in Fig. 7. $E_{\text{c.m.}}$/MeV = 69.0 (closed triangles), 51.4 (squares), 47.0 (open triangles), 40.6 (circles).

amount of energy dissipated when the fictitious particle moves between $q = 4.5$ and $q = 3.5$.

Moving q_0 closer to the barrier whose radius for the s wave is $q_{B0} = 1.43$ (see Table II) we see in Fig. 7(b) that the cross section starts to increase faster with $E_{\text{c.m.}}$. The reason for this is that a part of the trajectory, which, in fact, is dissipative, is not considered as such owing to Eq. (25). The increase of σ with the decrease of q_0 is larger at high values of $E_{\text{c.m.}}$ because the larger initial energy results in an earlier appearance of the dissipation. So, in all the calculations below we use $q_0 = 4.5$.

The capture conditions should be tuned as well as the initial conditions. The capture is supposed to happen at a particular value of the radial coordinate q_c (or R_c). In the TMSF without fluctuations it is usually assumed that capture happens if the fictitious particle overcomes the top of the Coulomb barrier [6,8] ($q_c = q_B$). Accounting for the thermal fluctuations makes the picture more complicated: After overcoming the barrier the fictitious particle can be scattered back with some probability. That is why in Ref. [9] the capture (no return) point is defined by the condition $dU_n/dR = 2$ MeV/fm; i.e., this point is positioned somewhat deeper beyond the barrier. This condition was founded only by the fit of the calculated capture cross sections to the data (see Fig. 2 of Ref. [9]). In the recent paper [16] the "touching" cross sections were calculated. From our point of view these are the same capture cross sections with the capture condition $q_c = q_t = 1$, i.e., $R_c = R_t = R_P + R_T$.

We assume the capture happens in one of the following two cases. First, two conditions must be fulfilled:

(i) the radial coordinate of the particle must become smaller than the particular share f_{cq} of the L-dependent barrier radius q_{BL},

$$q(t) < q_c = f_{cq} q_{BL}; \tag{26}$$

(ii) the radial kinetic energy must become of order of the temperature:

$$p^2(t)/(2m_q) < f_{cE}\theta(t). \tag{27}$$

The second case is when the trajectory penetrates beyond the barrier significantly deeper than in the first case:

$$q(t) < q_c = 0.5(q_t + q_{BL}). \tag{28}$$

This condition works if we make the strength coefficient of the radial friction very small.

We varied the coefficient f_{cE} between 1 and 2, and the coefficient f_{cq} between 0.94 and 1.00 and found that the calculated excitation functions did not change. Thus, in all the calculations below the values $f_{cE} = 1$ and $f_{cq} = 0.98$ are used.

III. TESTING THE MODEL

A. The influence of the friction strength coefficients

The calculated values of the cross sections depend upon the method of computing (either the BPM or the TMSF). In the latter case, for the given potential, the cross sections depend upon the friction strength coefficients K_R and K_φ. This subsection is devoted to studying this influence. Reaction $^{16}\text{O} + ^{92}\text{Zr}$ has been chosen as an example. Results are shown in Fig. 9.

The influence of the variation of the tangential friction strength on the results of the trajectory calculations was studied in Ref. [6]. However, in that work the range of the angular momenta which is interesting for us ($L < 80$) is not even shown (see Fig. 21 of Ref. [6]). The capture excitation functions calculated at different values of K_φ ranging from 10^{-5} MeV^{-1} zs up to 10^{-2} MeV^{-1} zs are presented in Fig. 9(a). The excitation function calculated using the nondissipative BPM is shown there too. It is seen that the reduction of K_φ from its standard value 10^{-4} MeV^{-1} zs does not influence the excitation function. Enhancing K_φ results in the slight increase of the cross section which is qualitatively correct. However, quantitatively this effect is very weak: The two orders of magnitude variation of K_φ results in an alternation of L_c by several units (typically from 1 to 3). This insensitivity of the capture cross sections to the value of K_φ was discussed recently in Ref. [16]. Thus, we fix $K_\varphi = 10^{-4}$ MeV^{-1} zs in all the calculations below.

The capture excitation functions calculated at different values of K_R are presented in Fig. 9(b). The excitation function calculated using the nondissipative BPM is shown there too (the curve with solid triangles up). It provides the upper limit which is reached in the dynamical calculations at $K_R = 10^{-3}$ MeV^{-1} zs (the curve with squares). It seems to us to be of importance that calculating the cross sections within the framework of the quantum BPM and the classical trajectory

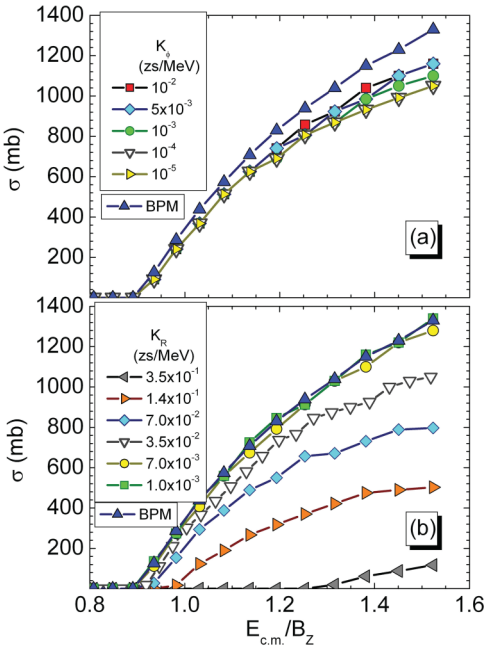

FIG. 9. (Color online) The influence of the coefficients K_φ (a) and K_R (b) on the fusion cross section for the reaction $^{16}O + ^{92}Zr$ (calculations are performed with the GK approximation of the DF2 potential; see Table II). In the upper panel $K_R = 3.5 \times 10^{-2}$ zs MeV^{-1}, in the lower panel $K_\phi = 1.0 \times 10^{-4}$ zs MeV^{-1}.

model without dissipation but with an absorptive border inside the barrier results in the same excitation functions. Increasing the value of K_R we suppress capture strongly, as expected. Thus, one can use the strength coefficient of the radial friction as a fit parameter if needed.

B. Comparing to the predecessors

Before comparing our results to the experimental data we consider that it is useful to make sure that our code reproduces the results of the previous theoretical works. We present the comparison with the results of Ref. [6] in Table V. It is pointed out in Ref. [6] that the standard parameter set of the GK potential [Eqs. (10)] provides good agreement with the experiment. However, in Ref. [6] these parameters had been adjusted individually for each reaction. Accounting for this remark we consider the agreement between the results of Ref. [6] and of our work to be reasonable.

TABLE V. Comparing our calculated capture cross section σ with those of Table 2 of Ref. [6].

Reaction	E_{lab} (MeV)	$E_{c.m.}$ (MeV)	σ(mb) [6]	σ(mb) (this work)
$^{84}Kr + ^{208}Pb$	718	511.45	522	473
	510	363.3	27	27
	494	351.9	0	0
$^{136}Xe + ^{209}Bi$	1130	684.55	198	89
$^{136}Xe + ^{165}Ho$	1130	619.4	440	343

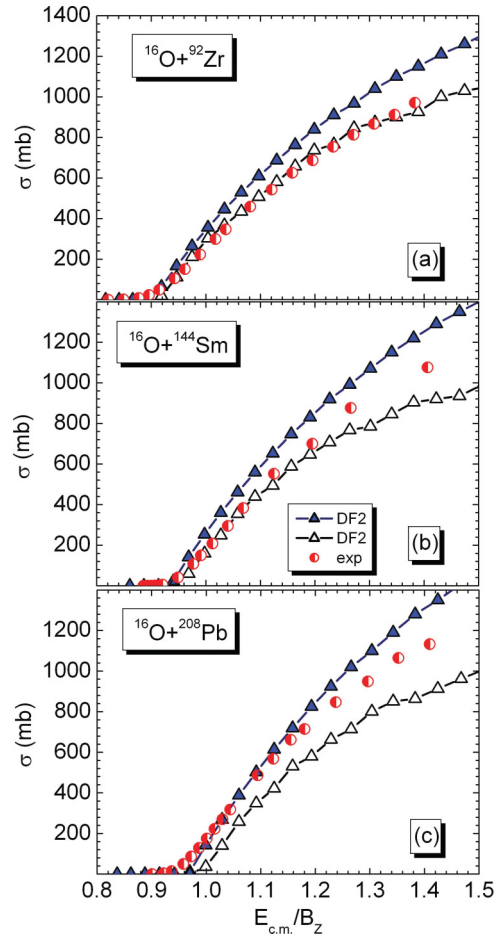

FIG. 10. (Color online) The fusion excitation functions calculated using the TMSF with the DF2 potentials (the curves with open triangles) are compared with the same experimental data as in Fig. 6 (semiopen circles). The results of the BPM with the same DF2 potentials are shown as well (the curves with solid triangles). The parameters of the potentials are shown in Tables II–IV.

The second comparison is made with the results of Ref. [8] and presented in Table VI, the compared quantities are the dissipative barrier energies B_{diss}, i.e., the values of $E_{c.m.}$ at which the dissipative trajectory with $L = 0$ is captured. Let us remind the reader that in contradistinction to Ref. [8] in our calculations the deformations of both reagents are not taken into account. Another difference is that we do not make an approximation of the results of the single folding calculations for each reaction: We use the standard parameter set of the GK

TABLE VI. Comparing our calculated dissipative barrier energies B_{diss} with those of Table 1 of Ref. [8].

Reaction	B_{exp} (MeV) [8]	B_{diss} (MeV) [8]	B_{diss} (MeV) (this work)
$^{40}Ar + ^{206}Pb$	162 ± 3	166.6	166.5
$^{64}Ni + ^{208}Pb$	264.5	265.9	266.6
$^{52}Cr + ^{208}Pb$	209.5	227.8	227.5
$^{50}Ti + ^{209}Bi$	190 ± 3	207.2	206.9
$^{50}Ti + ^{208}Pb$	191 ± 3	204.2	203.9

TABLE VII. Parameters of the DF2 potential for the system $^{16}O + ^{208}Pb$ displayed in Figs. 11 and 12.

Potential	q_{B0}	R_{B0} (fm)	U_{B0} (MeV)	Parameters of the potential	
DF2	1.27	11.75	75.28	$R_P = 2.608$ fm, $a_P = 0.465$ fm $R_T = 6.631$ fm, $a_T = 0.616$ fm	$A_0 = 20.0$ MeV, $A_1 = 4.0$ MeV, $A_2 = 4.8$ MeV, $r_0 = 1.34$ fm, $a = 0.52$ fm

potential [Eqs. (10)]. The third difference is that the capture conditions do not coincide. Accounting for these differences, the agreement between our dissipative barrier energies and the ones from Ref. [8] is surprisingly good.

IV. RESULTS

We calculated the capture excitation functions mostly within the framework of the classical dissipative trajectory model using Eq. (23). Sometimes for comparison we show the cross sections resulting from the BPM [Eqs. (22) and (24)]. As the first iteration we apply the friction strength coefficients ($K_R = 3.5 \times 10^{-2}$ MeV^{-1} zs, $K_\varphi = 1.0 \times 10^{-4}$ MeV^{-1} zs) which were found in Ref. [8] with the symmetrized single-folding potential. Remember that the GK formula is always used as the approximation of the DF2 potential.

Results of this first iteration are presented in Fig. 10. Before discussing these results let us mention the slight irregularities in our calculated excitation functions. These irregularities are discussed in the Appendix and should not distract the reader.

Note first the evidence of the apparently large diffuseness problem: The cross sections resulting from the BPM (the curves with solid triangles) are significantly above the data (semiopen circles). The cross sections calculated dynamically

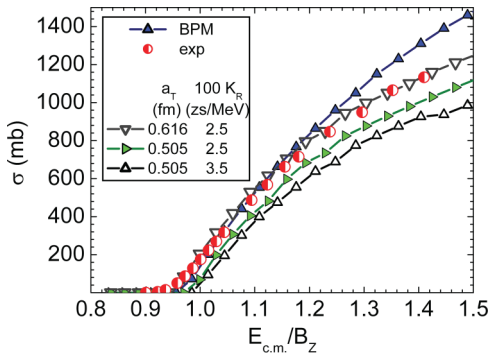

FIG. 11. (Color online) The fusion excitation functions for the $^{16}O + ^{208}Pb$ reaction with the modified radial dissipation strength coefficient K_R and matter density target diffuseness a_T. The curve with open triangles up corresponds to our original calculations ($a_T = 0.505$ fm, $K_R = 3.5 \times 10^{-2}$ MeV^{-1} zs); the curve with solid triangles right shows the result of the calculation with the reduced radial friction coefficient; the curve with open triangles down corresponds to the calculation with the additional increase of a_T. The results of the BPM (the curve with solid triangles up) and the experimental data (semiopen circles) are shown as well.

(the curves with open triangles) are in good agreement with the data for the lightest target nucleus. For the heavier target nuclei this agreement is destroyed: The results of the trajectory calculations are significantly below the data at high energies. Moreover, in the case of lead it looks like the capture barrier in the dynamical calculations is shifted up compared to the experimental one.

Thus, we try to vary the most uncertain parameters for the reaction $^{16}O + ^{208}Pb$: the radial dissipation strength coefficient K_R and the matter density diffuseness a_T. The coefficient K_φ is not varied because we have seen that it does not influence the calculated cross sections in our range of the collision energy. Reducing the radial friction is expected to elevate the excitation function especially at high energies. Such reduction is even expected because the value $K_R = 3.5 \times 10^{-2}$ MeV^{-1} zs was obtained in Ref. [8] with the single-folding (GK) potential, whereas the DF2 potential is significantly steeper and provides higher friction [see Fig. 4 and Eq. (5a)]. Increasing a_T should move the whole curve left owing to the reduction of the Coulomb barrier.

Results of the variations of K_R and a_T are displayed in Fig. 11. We see that reducing K_R from 3.5×10^{-2} MeV^{-1} zs to 2.5×10^{-2} MeV^{-1} zs and increasing simultaneously a_T from the initial value 0.505 to 0.616 fm brings the calculated capture excitation function to the satisfactory agreement with the data.

Now we keep the new value $K_R = 2.5 \times 10^{-2}$ MeV^{-1} zs and calculate again the cross sections for $^{16}O + ^{92}Zr$ and $^{16}O + ^{144}Sm$. The results are compared with the data in Fig. 12. We believe that this amount of agreement proves that the longstanding problem of the apparently large diffuseness of the SnnP can be solved within the framework of the classical dissipative trajectory model using the surface friction and the DF potential. Let us stress that this potential possesses a small diffuseness no matter what version of it is applied. Future development of the model (for instance, taking into account the dynamical deformations and fluctuations) can, of course, influence the value of the radial friction strength.

V. CONCLUSIONS

The extensive analysis of a vast set of data on precision capture excitation functions, in particular when both the projectile and the target nuclei are spherical, performed in Ref. [1] resulted in the problem of the apparently large diffuseness of the Woods-Saxon (WS) nucleus-nucleus strong interaction potential (SnnP). The potential was needed to fit the data at the collision energies well above the Coulomb barrier, where couplings to the vibrational states are of no importance.

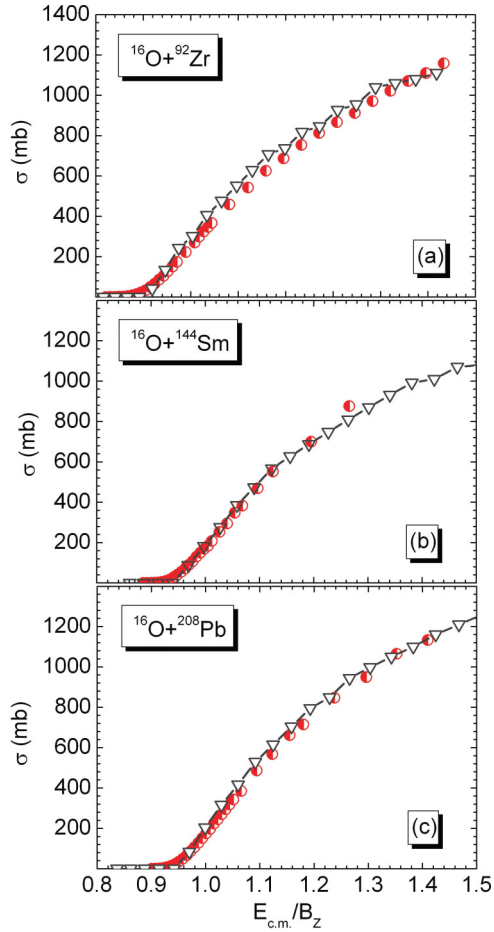

FIG. 12. (Color online) The fusion excitation functions calculated using the TMSF with the DF2 potential and $K_R = 2.5 \times 10^{-2}$ MeV^{-1} zs (the curves with triangles) are compared with the same experimental data as in Figs. 6 and 10 (semiopen circles). The parameters of the potentials are shown in Tables II, III, and VII.

The diffusenesses were much larger (about 1 fm) than those of the potentials used to fit the elastic scattering data (about 0.6 fm). In the present work we have undertaken an effort to see whether the problem is not in the potential itself but in the dynamical character of the collision process. Dissipation is the first dynamical effect which must be accounted for.

Therefore, we constructed a classical dissipative trajectory model within the framework of which we tried to reproduce the data on fusion (capture) of ^{16}O with ^{92}Zr, ^{144}Sm, and ^{208}Pb. Our model resembles very much the one of Ref. [6]. However, the models are different to a certain extent.

First, the models use the different potentials. In our case this is the double-folding potential with the density-dependent M3Y *NN* forces with the finite radius of the exchange part. Let us stress that this potential possesses a small diffuseness of about 0.6 fm. For making dynamical modeling of the collision process the DF potential must be approximated by an analytical expression. We found that the Gross-Kalinowski profile [see Eqs. (8) and (9)] serves for this purpose significantly better than the conventional WS formula (1) used in Ref. [1].

Second, in Ref. [6] a comparison was done with the data whose accuracy was never better than 10%, whereas we compare our calculation results with the data of 1% accuracy. This circumstance forced us to tune very carefully all the parameters of the model like, e.g., the entrance point.

It is worth that because varying slightly the strength of radial friction (universally for all three reactions) and the diffuseness of the matter density of ^{208}Pb we have obtained the satisfactory agreement of the calculated excitation functions with the data. We dare to say that this agreement can be considered as evidence that the old problem of the apparently large diffuseness of the SnnP is indeed an artifact related to the dynamics of the process.

It should be kept in mind that our classical calculations provide an approximate description for capture cross sections in very asymmetric systems above the Coulomb barrier. However, in the vicinity of the barrier mean trajectory calculations break down owing to fluctuation mechanisms arising from two different sources: (i) the diffusion mechanism associated with dissipation and (ii) the barrier fluctuations owing to coupling between relative motion and low-frequency surface vibrations (see, e.g., Ref. [32]).

APPENDIX

Here we discuss the jumps (or rather the kinks) exhibited by the cross sections calculated within the framework of the TMSF in Figs. 9–12. This sort of irregularity is typical for the trajectory calculations where the fluctuations are absent. To understand this let us inspect Eq. (23). As the collision energy increases, the first multiplier decreases in a continuous manner, whereas L_c and consequently the second multiplier abruptly increases by unity. The resulting kinks define the accuracy of the calculated cross sections in whatever classical trajectory model, provided L is considered as the discrete variable (which it is in reality) and fluctuations are ignored (this makes the model less realistic). To estimate the effect we performed the cross-section calculations using a small step in the energy. The results shown in Fig. 13 confirm our speculations.

It is expected that the quantum and thermal fluctuations smear out (or at least weaken) this structure. However, for lighter systems the structure seems to have been observed [24,31].

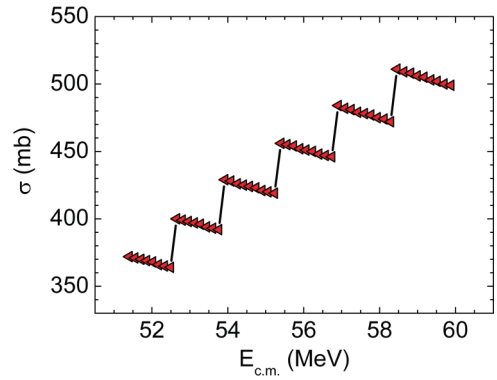

FIG. 13. (Color online) The capture excitation function for the system ^{16}O + ^{92}Zr calculated with the small $E_{c.m.}$ step in the framework of the TMSF [GK potential of Eqs. (8)–(10)].

[1] J. O. Newton, R. D. Butt, M. Dasgupta, D. J. Hinde, I. I. Gontchar, C. R. Morton, and K. Hagino, Phys. Lett. B **586**, 219 (2004); Phys. Rev. C **70**, 024605 (2004).
[2] http://nrv.jinr.ru/nrv/webnrv/fusion/reactions.php
[3] M. Dasgupta, D. J. Hinde, N. Rowley, and A. M. Stefanini, Annu. Rev. Nucl. Part. Sci. **48**, 401 (1998).
[4] K. Hagino, N. Rowley, and A. T. Kruppa, Comput. Phys. Commun. **123**, 143 (1999).
[5] P. Fröbrich and R. Lipperheide, *Theory of Nuclear Reactions*, Oxford Studies in Nuclear Physics, Vol. 18 (Oxford University Press, Oxford, 1996).
[6] D. H. E. Gross and H. Kalinowski, Phys. Rep. **45**, 175 (1978).
[7] P. Fröbrich, B. Strack, and M. Durand, Nucl. Phys. A **406**, 557 (1983).
[8] P. Fröbrich, Phys. Rep. **116**, 337 (1984).
[9] J. Marten and P. Fröbrich, Nucl. Phys. A **545**, 854 (1992).
[10] P. Fröbrich and I. I. Gontchar, Phys. Rep. **292**, 131 (1998).
[11] Dao T. Khoa, G. R. Satchler, and W. von Oertzen, Phys. Rev. C **56**, 954 (1997).
[12] I. I. Gontchar and M. V. Chushnyakova, Comput. Phys. Commun. **181**, 168 (2010).
[13] J. O. Newton, C. R. Morton, M. Dasgupta, J. R. Leigh, J. C. Mein, D. J. Hinde, H. Timmers, and K. Hagino, Phys. Rev. C **64**, 064608 (2001).
[14] J. R. Leigh, M. Dasgupta, D. J. Hinde, J. C. Mein, C. R. Morton, R. C. Lemmon, J. P. Lestone, J. O. Newton, H. Timmers, J. X. Wei, and N. Rowley, Phys. Rev. C **52**, 3151 (1995).
[15] C. R. Morton, A. C. Berriman, M. Dasgupta, D. J. Hinde, J. O. Newton, K. Hagino, and I. J. Thompson, Phys. Rev. C **60**, 044608 (1999).
[16] T. I. Nevzorova and G. I. Kosenko, Phys. At. Nucl. **71**, 1373 (2008).
[17] A. V. Ignatyuk, M. G. Itkis, V. N. Okolovich, G. N. Smirenkin, and A. S. Tishin, Yad. Fiz. **21**, 1185 (1975).
[18] H. J. Krappe and K. Pomorski, *Theory of Nuclear Fission*, Lecture Notes in Physics, Vol. 838 (Springer-Verlag, Berlin, Heidelberg, 2012).
[19] I. I. Gontchar, M. Dasgupta, D. J. Hinde, and J. O. Newton, Phys. Rev. C **69**, 024610 (2004).
[20] N. Anantaraman, H. Toki, and G. F. Bertsch, Nucl. Phys. A **398**, 269 (1983).
[21] H. de Vries, C. W. de Jager, and C. de Vries, At. Data Nucl. Data Tables **36**, 495 (1987).
[22] Ş. Mişicu and W. Greiner, Phys. Rev. C **66**, 044606 (2002).
[23] V. I. Zagrebaev, A. V. Karpov, Y. Aritomo, M. A. Naumenko, and W. Greiner, Phys. Elem. Part. At. Nucl. **38**, 892 (2007).
[24] H. Esbensen, Phys. Rev. C **77**, 054608 (2008).
[25] M. Ismail, A. Y. Ellithi, M. M. Botros, and A. E. Mellik, Phys. Rev. C **75**, 064610 (2007).
[26] O. N. Ghodsi and V. Zanganeh, Phys. Rev. C **79**, 044604 (2009).
[27] O. N. Ghodsi and R. Gharaei, Phys. Rev. C **84**, 024612 (2011).
[28] D. T. Khoa and W. von Oertzen, Phys. Rev. B **304**, 8 (1993).
[29] E. Uegaki and Y. Abe, Progr. Theor. Phys. **90**, 615 (1993).
[30] D. L. Hill and J. A. Wheeler, Phys. Rev. **89**, 1102 (1953).
[31] I. Tserruya, Y. Eisen, D. Pelte, A. Gavron, H. Oeschler, D. Berndt, and H. L. Harney, Phys. Rev. C **18**, 1688 (1978).
[32] S. Ayik, B. Yilmaz, and D. Lacroix, Phys. Rev. C **81**, 034605 (2010).